On sixfold coupled buckling of thin-walled composite beams

Thuc Phuong Vo* and Jaehong Lee†
Department of Architectural Engineering, Sejong University
98 Kunja Dong, Kwangjin Ku, Seoul 143-747, Korea

(Dated: March 12, 2009)

A general analytical model based on shear-deformable beam theory has been developed to study the flexural-torsional coupled buckling of thin-walled composite beams with arbitrary lay-ups under axial load. This model accounts for all the structural coupling coming from the material anisotropy. The seven governing differential equations for coupled flexural-torsional-shearing buckling are derived. The resulting coupling is referred to as sixfold coupled buckling. Numerical results are obtained for thin-walled composite beams to investigate effects of shear deformation, fiber orientation and modulus ratio on the critical buckling loads and corresponding mode shapes.

Keywords: Thin-walled composite beams; shear deformation; flexural-torsional-shearing buckling.

I. INTRODUCTION

Fiber-reinforced plastics (FRP) have been used over the past few decades in a variety of structures. Composites have many desirable characteristics, such as high ratio of stiffness and strength to weight, corrosion resistance and magnetic transparency. Thin-walled structural shapes made up of composite materials, which are usually produced by pultrusion, are being increasingly used in many engineering fields. However, the structural behavior is very complex due to coupling effects as well as warping-torsion and thus, the accurate prediction of stability limit state and dynamic characteristics is of the fundamental importance in the design of thin-walled composite structures.

The theory of thin-walled open section members made of isotropic materials was first developed by Vlasov [1] and Gjelsvik [2]. Up to the present, investigation into the stability behavior of these members has received widespread attention and has been carried out extensively. Closed-form solution for flexural and torsional buckling of isotropic thin-walled beams are found in the literature (Timoshenko [3], Trahair [4]). For thin-walled composite beams, the flexural and torsional buckling are fully coupled even for a doubly symmetric cross-section due to their material anisotropy. Based on a Vlasov-type linear hypothesis, Pandey et al. [5] investigated flexural-torsional stability of thin-walled composite I-section beams. A finite element having seven degrees of freedom at each node was developed

---

*Graduate student

†Professor, corresponding author. Tel.:+82-2-3408-3287; fax:+82-2-3408-3331

; Electronic address: `jhlee@sejong.ac.kr`

by Lin et al. [6] to study the stability problem of thin-walled composite beams. The influence of the in plane shear strain on the stability of the members was considered. Shield and Morey [7] developed a new theory for analysis buckling of composite beams of open and closed cross section. The theory took into account deformation in the plane of the cross section due to anticlastic curvature. Kollar [8-10] focused on the analysis of flexural-torsional buckling and vibration of thin-walled open section composite beams. Vlasov's classical theory of thin-walled beams was modified to include both the transverse shear and the restrained warping induced shear deformations. The works of Davalos, Qiao and coworkers [11-13] deserved special attention because they presented a comprehensive experimental and analytical approach to study flexural-torsional buckling behavior of full-size pultruded FRP I-beams and channel section. An energy method based on nonlinear plate theory was developed for instability of FRP beams and the formulation included shear effect and bending-twisting coupling. The monograph of Librescu and Song [14] was concerned not only with the foundation and formulation of modern linear and nonlinear theories of thin-walled composite beams but also provided powerful mathematical tools to address issues of statics and dynamics of these members. Cortinez, Piovan, Machado and coworkers [15-18] introduced a new theoretical model for the generalized linear analysis of thin-walled composite beams. This model allowed studying many problems of static's, free vibrations with or without arbitrary initial stresses and linear stability of composite thin-walled beams. In their research [15-18], thin-walled composite beams for both open and closed cross-sections and the shear flexibility (bending, non-uniform warping) were incorporated. However, it was strictly valid for symmetric balanced laminates and especially orthotropic laminates. Back and Will [19] developed a shear-flexible finite element based on an orthogonal Cartesian coordinate system for the flexural and buckling analyses of thin-walled composite I-beams with both doubly and mono-symmetrical cross-sections. Using the first-order shear deformable beam theory, the beam element included both the transverse shear and restrained warping were derived. Recently, a simple but efficient method to evaluate the exact element stiffness matrix was presented by Kim et al. [20,21] in order to perform the spatially coupled stability analysis of thin-walled composite beams with symmetric and arbitrary laminations under a compressive force.

In this paper, which is an extension of the authors' previous works [22-25], flexural-torsional coupled buckling of thin-walled composite beams with arbitrary lay-ups is presented. This model is based on the first-order shear-deformable beam theory, and accounts for all the structural coupling coming from the material anisotropy. The seven governing differential equations for coupled flexural-torsional-shearing buckling are derived. Numerical results are obtained to investigate the effects of fiber angle, span-to-height ratio and modulus ratio on the critical buckling loads and corresponding mode shapes of thin-walled composite beams.

II. KINEMATICS

The theoretical developments presented in this paper require two sets of coordinate systems which are mutually interrelated. The first coordinate system is the orthogonal Cartesian coordinate system (x, y, z), for which the x and y axes lie in the plane of the cross section and the z axis parallel to the longitudinal axis of the beam. The second coordinate system is the local plate coordinate (n, s, z) as shown in Fig.1, wherein the n axis is normal to the middle surface of a plate element, the s axis is tangent to the middle surface and is directed along the contour line of the cross section. The (n, s, z) and (x, y, z) coordinate systems are related through an angle of orientation θ as defined in Fig.1. Point P is called the pole axis, through which the axis parallel to the z axis is called the pole axis.

To derive the analytical model for a thin-walled composite beam, the following assumptions are made:

1. The contour of the thin wall does not deform in its own plane.
2. Transverse shear strains $\gamma^\circ_{xz}, \gamma^\circ_{yz}$ and warping shear γ°_ω are incorporated. It is assumed that they are uniform over the cross-sections.
3. Each laminate is thin and perfectly bonded.
4. Local buckling is not considered.

According to assumption 1, the midsurface displacement components $\bar{u}, \bar{v}$ at a point A in the contour coordinate system can be expressed in terms of a displacements U, V of the pole P in the x, y directions, respectively, and the rotation angle Φ about the pole axis,

$$\bar{u}(s,z) = U(z)\sin\theta(s) - V(z)\cos\theta(s) - \Phi(z)q(s) \tag{1a}$$

$$\bar{v}(s,z) = U(z)\cos\theta(s) + V(z)\sin\theta(s) + \Phi(z)r(s) \tag{1b}$$

These equations apply to the whole contour. The out-of-plane shell displacement $\bar{w}$ can now be found from the assumption 2. For each element of middle surface, the midsurface shear strains in the contour can be expressed with respect to the transverse shear and warping shear strains.

$$\bar{\gamma}_{nz}(s,z) = \gamma^\circ_{xz}(z)\sin\theta(s) - \gamma^\circ_{yz}(z)\cos\theta(s) - \gamma^\circ_\omega(z)q(s) \tag{2a}$$

$$\bar{\gamma}_{sz}(s,z) = \gamma^\circ_{xz}(z)\cos\theta(s) + \gamma^\circ_{yz}(z)\sin\theta(s) + \gamma^\circ_\omega(z)r(s) \tag{2b}$$

Further, it is assumed that midsurface shear strain in $s - n$ direction is zero $(\bar{\gamma}_{sn} = 0)$. From the definition of the shear strain, $\bar{\gamma}_{sz} = 0$ can also be given for each element of middle surface as:

$$\bar{\gamma}_{sz}(s,z) = \frac{\partial \bar{v}}{\partial z} + \frac{\partial \bar{w}}{\partial s} \tag{3}$$

After substituting for $\bar{v}$ from Eq.(1) into Eq.(3) and considering the following geometric relations,

$$dx = ds\cos\theta \tag{4a}$$

$$dy = ds\sin\theta \tag{4b}$$

Displacement $\bar{w}$ can be integrated with respect to s from the origin to an arbitrary point on the contour,

$$\bar{w}(s,z) = W(z) + \Psi_y(z)x(s) + \Psi_x(z)y(s) + \Psi_\omega(z)\omega(s) \tag{5}$$

where Ψ_x, Ψ_y and Ψ_ω represent rotations of the cross section with respect to x, y and ω, respectively, given by:

$$\Psi_y = \gamma_{xz}^{\circ}(z) - U' \tag{6a}$$

$$\Psi_x = \gamma_{yz}^{\circ}(z) - V' \tag{6b}$$

$$\Psi_\omega = \gamma_{\omega}^{\circ}(z) - \Phi' \tag{6c}$$

When the transverse shear effect is ignored, Eq.(6) degenerates to $\Psi_y = -U'$, $\Psi_x = -V'$ and $\Psi_\omega = -\Phi'$. As a result, the number of unknown variables reduces to four leading to the Euler-Bernoulli beam model. The prime ($'$) is used to indicate differentiation with respect to z; and ω is the so-called sectorial coordinate or warping function given by

$$\omega(s) = \int_{s_\circ}^{s} r(s)ds \tag{7a}$$

The displacement components u, v, w representing the deformation of any generic point on the profile section are given with respect to the midsurface displacements $\bar{u}, \bar{v}, \bar{w}$ by assuming the first order variation of inplane displacements v, w through the thickness of the contour as:

$$u(s,z,n) = \bar{u}(s,z) \tag{8a}$$

$$v(s,z,n) = \bar{v}(s,z) + n\bar{\psi}_s(s,z) \tag{8b}$$

$$w(s,z,n) = \bar{w}(s,z) + n\bar{\psi}_z(s,z) \tag{8c}$$

where, $\bar{\psi}_s$ and $\bar{\psi}_z$ denote the rotations of a transverse normal about the z and s axis, respectively. These functions can be determined by considering that the midsurface shear strains γ_{nz} is given by definition:

$$\bar{\gamma}_{nz}(s,z) = \frac{\partial \bar{w}}{\partial n} + \frac{\partial \bar{u}}{\partial z} \tag{9}$$

By comparing Eq.(2) and (9), the function can $\bar{\psi}_z$ can be written as

$$\bar{\psi}_z = \Psi_y \sin\theta - \Psi_x \cos\theta - \Psi_\omega q \tag{10}$$

Similarly, using the assumption that the shear strain γ_{sn} should vanish at midsurface, the function $\bar{\psi}_s$ can be obtained

$$\bar{\psi}_s = -\frac{\partial \bar{u}}{\partial s} \tag{11}$$

The strains associated with the small-displacement theory of elasticity are given by

$$\epsilon_s(s,z,n) = \bar{\epsilon}_s(s,z) + n\bar{\kappa}_s(s,z) \tag{12a}$$

$$\epsilon_z(s,z,n) = \bar{\epsilon}_z(s,z) + n\bar{\kappa}_z(s,z) \tag{12b}$$

$$\gamma_{sz}(s,z,n) = \bar{\gamma}_{sz}(s,z) + n\bar{\kappa}_{sz}(s,z) \tag{12c}$$

$$\gamma_{nz}(s,z,n) = \bar{\gamma}_{nz}(s,z) + n\bar{\kappa}_{nz}(s,z) \tag{12d}$$

where

$$\bar{\epsilon}_s = \frac{\partial \bar{v}}{\partial s}; \quad \bar{\epsilon}_z = \frac{\partial \bar{w}}{\partial z} \tag{13a}$$

$$\bar{\kappa}_s = \frac{\partial \bar{\psi}_s}{\partial s}; \quad \bar{\kappa}_z = \frac{\partial \bar{\psi}_z}{\partial z} \tag{13b}$$

$$\bar{\kappa}_{sz} = \frac{\partial \bar{\psi}_z}{\partial s} + \frac{\partial \bar{\psi}_s}{\partial z}; \quad \bar{\kappa}_{nz} = 0 \tag{13c}$$

All the other strains are identically zero. In Eq.(13), $\bar{\epsilon}_s$ and $\bar{\kappa}_s$ are assumed to be zero, and $\bar{\epsilon}_z$, $\bar{\kappa}_z$ and $\bar{\kappa}_{sz}$ are midsurface axial strain and biaxial curvature of the shell, respectively. The above shell strains can be converted to beam strain components by substituting Eqs.(1), (5) and (8) into Eq.(13) as

$$\bar{\epsilon}_z = \epsilon_z^\circ + x\kappa_y + y\kappa_x + \omega\kappa_\omega \tag{14a}$$

$$\bar{\kappa}_z = \kappa_y \sin\theta - \kappa_x \cos\theta - \kappa_\omega q \tag{14b}$$

$$\bar{\kappa}_{sz} = \kappa_{sz} \tag{14c}$$

where $\epsilon_z^\circ, \kappa_x, \kappa_y, \kappa_\omega$ and κ_{sz} are axial strain, biaxial curvatures in the x and y direction, warping curvature with respect to the shear center, and twisting curvature in the beam, respectively defined as

$$\epsilon_z^\circ = W' \tag{15a}$$

$$\kappa_x = \Psi_x' \tag{15b}$$

$$\kappa_y = \Psi_y' \tag{15c}$$

$$\kappa_\omega = \Psi_\omega' \tag{15d}$$

$$\kappa_{sz} = \Phi' - \Psi_\omega \tag{15e}$$

The resulting strains can be obtained from Eqs.(12) and (14) as

$$\epsilon_z = \epsilon_z^\circ + (x + n\sin\theta)\kappa_y + (y - n\cos\theta)\kappa_x + (\omega - nq)\kappa_\omega \tag{16a}$$

$$\gamma_{sz} = \gamma_{xz}^\circ \cos\theta + \gamma_{yz}^\circ \sin\theta + \gamma_\omega^\circ r + n\kappa_{sz} \tag{16b}$$

$$\gamma_{nz} = \gamma_{xz}^\circ \sin\theta - \gamma_{yz}^\circ \cos\theta - \gamma_\omega^\circ q \tag{16c}$$

III. VARIATIONAL FORMULATION

The total potential energy of the system can be stated, in its buckled shape, as

$$\Pi = \mathcal{U} + \mathcal{V} \tag{17}$$

where $\mathcal{U}$ is the strain energy

$$\mathcal{U} = \frac{1}{2}\int_v (\sigma_z\epsilon_z + \sigma_{sz}\gamma_{sz} + \sigma_{nz}\gamma_{nz})dv \tag{18}$$

After substituting Eq.(16) into Eq.(18)

$$\begin{aligned}\mathcal{U} &= \frac{1}{2}\int_v \Big\{\sigma_z\Big[\epsilon_z^\circ + (x + n\sin\theta)\kappa_y + (y - n\cos\theta)\kappa_x + (\omega - nq)\kappa_\omega\Big] \\ &+ \sigma_{sz}\Big[\gamma_{xz}^\circ\cos\theta + \gamma_{yz}^\circ\sin\theta + \gamma_\omega^\circ r + n\kappa_{sz}\Big] + \sigma_{nz}\Big[\gamma_{xz}^\circ\sin\theta - \gamma_{yz}^\circ\cos\theta + \gamma_\omega^\circ q\Big]\Big\}dv\end{aligned} \tag{19}$$

The variation of strain energy, Eq.(19), can be stated as

$$\delta\mathcal{U} = \int_0^l (N_z\delta\epsilon_z + M_y\delta\kappa_y + M_x\delta\kappa_x + M_\omega\delta\kappa_\omega + V_x\delta\gamma_{xz}^\circ + V_y\delta\gamma_{yz}^\circ + T\delta\gamma_\omega^\circ + M_t\delta\kappa_{sz})dz \tag{20}$$

where $N_z, M_x, M_y, M_\omega, V_x, V_y, T, M_t$ are axial force, bending moments in the x- and y-directions, warping moment (bimoment), and torsional moment with respect to the centroid, respectively, defined by integrating over the cross-sectional area A as

$$N_z = \int_A \sigma_z dsdn \tag{21a}$$

$$M_y = \int_A \sigma_z (x + n\sin\theta) dsdn \tag{21b}$$

$$M_x = \int_A \sigma_z (y - n\cos\theta) dsdn \tag{21c}$$

$$M_\omega = \int_A \sigma_z (\omega - nq) dsdn \tag{21d}$$

$$V_x = \int_A (\sigma_{sz}\cos\theta + \sigma_{nz}\sin\theta) dsdn \tag{21e}$$

$$V_y = \int_A (\sigma_{sz}\sin\theta - \sigma_{nz}\cos\theta) dsdn \tag{21f}$$

$$T = \int_A (\sigma_{sz} r + \sigma_{nz} q) dsdn \tag{21g}$$

$$M_t = \int_A \sigma_{sz} n dsdn \tag{21h}$$

The potential of in-plane loads $\mathcal{V}$ due to transverse deflection

$$\mathcal{V} = \frac{1}{2}\int_v \overline{\sigma}_z^0 \Big[(u')^2 + (v')^2\Big] dv \tag{22}$$

where $\overline{\sigma}_z^0$ is the averaged constant in-plane edge axial stress, defined by $\overline{\sigma}_z^0 = P^0/A$. The variation of the potential of in-plane loads at the centroid is expressed by substituting the assumed displacement field into Eq.(22) as

$$\begin{aligned} \delta\mathcal{V} &= \int_v \frac{P^0}{A}\Big[U'\delta U' + V'\delta V' + (q^2 + r^2 + 2rn + n^2)\Phi'\delta\Phi' + (\Phi'\delta U' + U'\delta\Phi')\big[n\cos\theta - (y - y_p)\big] \\ &+ (\Phi'\delta V' + V'\delta\Phi')\big[n\cos\theta + (x - x_p)\big]\Big] dv \end{aligned} \tag{23}$$

The kinetic energy of the system is given by

$$\mathcal{T} = \frac{1}{2}\int_v \rho(\dot{u}^2 + \dot{v}^2 + \dot{w}^2) dv \tag{24}$$

where ρ is a density.

The variation of the kinetic energy is expressed by substituting the assumed displacement field into Eq.(24) as

$$
\begin{aligned}
\delta\mathcal{T} \;=\; & \int_v \rho \Bigg\{ \delta\dot{W}\Big[\dot{W}+\dot{\Psi}_x(y-n\cos\theta)+\dot{\Psi}_y(x+n\sin\theta)+\dot{\Psi}_\omega(\omega-nq)\Big] \\
+\; & \delta\dot{U}\Big[\dot{U}+\dot{\Phi}\big[n\cos\theta-(y-y_p)\big]\Big]+\delta\dot{V}\Big[m_0\dot{V}+\dot{\Phi}\big[n\sin\theta+(x-x_p)\big]\Big] \\
+\; & \delta\dot{\Phi}\dot{\Phi}\Big[\dot{U}\big[n\cos\theta-(y-y_p)\big]+\dot{V}\big[n\sin\theta+(x-x_p)\big]+\dot{\Phi}(q^2+r^2+2rn+n^2)\Big] \\
+\; & \delta\dot{\Psi}_x\dot{\Psi}_x\Big[\dot{W}(y-n\cos\theta)+\dot{\Psi}_x(y-n\cos\theta)^2+\dot{\Psi}_y(x+n\sin\theta)(y-n\cos\theta)+\dot{\Psi}_\omega(y-n\cos\theta)(\omega-nq)\Big] \\
+\; & \delta\dot{\Psi}_y\dot{\Psi}_y\Big[\dot{W}(x+n\sin\theta)+\dot{\Psi}_x(x+n\sin\theta)(y-n\cos\theta)+\dot{\Psi}_y(x+n\sin\theta)^2+\dot{\Psi}_\omega(x+n\sin\theta)(\omega-nq)\Big] \\
+\; & \delta\dot{\Psi}_\omega\dot{\Psi}_\omega\Big[\dot{W}(\omega-nq)+\dot{\Psi}_x(y-n\cos\theta)(\omega-nq)+\dot{\Psi}_y(x+n\sin\theta)(\omega-nq)+\dot{\Psi}_\omega(\omega-nq)^2\Big]\Bigg\}dv
\end{aligned}
\tag{25}
$$

In Eqs.(23) and (25), the following geometric relations are used (Fig.1)

$$x-x_p \;=\; q\cos\theta+r\sin\theta \tag{26a}$$

$$y-y_p \;=\; q\sin\theta-r\cos\theta \tag{26b}$$

In order to derive the equations of motion, Hamilton's principle is used

$$\delta\int_{t_1}^{t_2}(\mathcal{T}-\Pi)dt \;=\; 0 \tag{27}$$

Substituting Eqs.(20), (23) and (25) into Eq.(27), the following weak statement is obtained

$$
\begin{aligned}
0 \;=\; & \int_{t_1}^{t_2}\int_0^l \Big\{\delta\dot{W}\big[m_0\dot{W}-m_c\dot{\Psi}_x+m_s\dot{\Psi}_y+(m_\omega-m_q)\dot{\Psi}_\omega\big]+\delta\dot{U}\big[m_0\dot{U}+(m_c+y_pm_0)\dot{\Phi}\big] \\
+\; & \delta\dot{V}\big[m_0\dot{V}+(m_s-x_pm_0)\dot{\Phi}\big]+\delta\dot{\Phi}\big[(m_c+y_pm_0)\dot{U}+(m_s-x_pm_0)\dot{V}+(m_p+m_2+2m_r)\dot{\Phi}\big] \\
+\; & \delta\dot{\Psi}_x\big[-m_c\dot{W}+(m_{y2}-2m_{yc}+m_{c2})\dot{\Psi}_x+(m_{xycs}-m_{cs})\dot{\Psi}_y+(m_{y\omega}-m_{y\omega qc}+m_{qc})\dot{\Psi}_\omega\big] \\
+\; & \delta\dot{\Psi}_y\big[m_s\dot{W}+(m_{xycs}-m_{cs})\dot{\Psi}_x+(m_{x2}+2m_{xs}+m_{s2})\dot{\Psi}_y+(m_{x\omega}+m_{x\omega qs}-m_{qs})\dot{\Psi}_\omega\big] \\
+\; & \delta\dot{\Psi}_\omega\big[(m_\omega-m_q)\dot{W}+(m_{y\omega}-m_{y\omega qc}+m_{qc})\dot{\Psi}_x+(m_{x\omega}+m_{x\omega qs}-m_{qs})\dot{\Psi}_y+(m_{\omega 2}-2m_{q\omega}+m_{q2})\dot{\Psi}_\omega\big] \\
-\; & P^0\big[\delta U'(U'+\Phi'y_p)+\delta V'(V'-\Phi'x_p)+\delta\Phi'(\Phi'\frac{I_p}{A}+U'y_p-V'x_p)\big]-N_z\delta W' \\
-\; & M_y\delta\Psi_y'-M_x\delta\Psi_x'-M_\omega\delta\Psi_\omega'-V_x\delta(U'+\Psi_y)-V_y\delta(V'+\Psi_x)-T\delta(\Phi'-\Psi_\omega)-M_t\delta(\Phi'-\Psi_\omega)\Big\}dzdt
\end{aligned}
\tag{28}
$$

All the inertia coefficients in Eq.(28) are given in Ref.[24].

IV. CONSTITUTIVE EQUATIONS

The constitutive equations of a k^{th} orthotropic lamina in the laminate co-ordinate system of section are given by

$$\left\{\begin{array}{c}\sigma_z\\ \\ \sigma_{sz}\end{array}\right\}^k = \left[\begin{array}{cc}\bar{Q}^*_{11} & \bar{Q}^*_{16}\\ \\ \bar{Q}^*_{16} & \bar{Q}^*_{66}\end{array}\right]^k \left\{\begin{array}{c}\epsilon_z\\ \\ \gamma_{sz}\end{array}\right\} \tag{29}$$

where $\bar{Q}^*_{ij}$ are transformed reduced stiffnesses. The transformed reduced stiffnesses can be calculated from the transformed stiffnesses based on the plane stress ($\sigma_s = 0$) and plane strain ($\epsilon_s = 0$) assumption. More detailed explanation can be found in Ref.[26]

The constitutive relation for out-of-plane stress and strain is given by

$$\sigma_{nz} = \bar{Q}_{55}\gamma_{nz} \tag{30}$$

The constitutive equations for bar forces and bar strains are obtained by using Eqs.(16), (21) and (29)

$$\left\{\begin{array}{c}N_z\\ M_y\\ M_x\\ M_\omega\\ M_t\\ V_x\\ V_y\\ T\end{array}\right\} = \left[\begin{array}{cccccccc}E_{11} & E_{12} & E_{13} & E_{14} & E_{15} & E_{16} & E_{17} & E_{18}\\ & E_{22} & E_{23} & E_{24} & E_{25} & E_{26} & E_{27} & E_{28}\\ & & E_{33} & E_{34} & E_{35} & E_{36} & E_{37} & E_{38}\\ & & & E_{44} & E_{45} & E_{46} & E_{47} & E_{48}\\ & & & & E_{55} & E_{56} & E_{57} & E_{58}\\ & & & & & E_{66} & E_{67} & E_{68}\\ & & & & & & E_{77} & E_{78}\\ \text{sym.} & & & & & & & E_{88}\end{array}\right] \left\{\begin{array}{c}\epsilon^\circ_z\\ \kappa_y\\ \kappa_x\\ \kappa_\omega\\ \kappa_{sz}\\ \gamma^\circ_{xz}\\ \gamma^\circ_{yz}\\ \gamma^\circ_\omega\end{array}\right\} \tag{31}$$

where E_{ij} are stiffnesses of thin-walled composite beams and given in Ref.[23].

V. EQUATIONS OF MOTION

The equations of motion of the present study can be obtained by integrating the derivatives of the varied quantities by parts and collecting the coefficients of $\delta W, \delta U, \delta V, \delta\Phi, \delta\Psi_y, \delta\Psi_x$ and $\delta\Psi_\omega$

$$N_z' = m_0\ddot{W} - m_c\ddot{\Psi}_x + m_s\ddot{\Psi}_y + (m_\omega - m_q)\ddot{\Psi}_\omega \tag{32a}$$

$$V_x' + P^0\big(U'' + \Phi'' y_p\big) = m_0\ddot{U} + (m_c + y_p m_0)\ddot{\Phi} \tag{32b}$$

$$V_y' + P^0\big(V'' - \Phi'' x_p\big) = m_0\ddot{V} + (m_s - x_p m_0)\ddot{\Phi} \tag{32c}$$

$$M_t' + T' + P^0\big(\Phi''\frac{I_p}{A} + U'' y_p - V'' x_p\big) = (m_c - m_y + y_p m_0)\ddot{U} + (m_s - x_p m_0)\ddot{V} + (m_p + m_2 + 2m_r)\ddot{\Phi} \tag{32d}$$

$$M_y' - V_x = m_s\ddot{W} + (m_{xycs} - m_{cs})\ddot{\Psi}_x + (m_{x2} + 2m_{xs} + m_{s2})\ddot{\Psi}_y \tag{32e}$$

$$+ \ (m_{x\omega} + m_{x\omega qs} - m_{qs})\ddot{\Psi}_\omega \tag{32f}$$

$$M_x' - V_y = -m_c\ddot{W} + (m_{y2} - 2m_{yc} + m_{c2})\ddot{\Psi}_x + (m_{xycs} - m_{cs})\ddot{\Psi}_y \tag{32g}$$

$$+ \ (m_{y\omega} - m_{y\omega qc} + m_{qc})\ddot{\Psi}_\omega \tag{32h}$$

$$M_\omega' + M_t - T = (m_\omega - m_q)\ddot{W} + (m_{y\omega} - m_{y\omega qc} + m_{qc})\ddot{\Psi}_x \tag{32i}$$

$$+ \ (m_{x\omega} + m_{x\omega qs} - m_{qs})\ddot{\Psi}_y$$

$$+ \ (m_{\omega 2} - 2m_{q\omega} + m_{q2})\ddot{\Psi}_\omega \tag{32j}$$

The natural boundary conditions are of the form

$$\delta W \ : \quad W = \overline{W}_0 \quad \text{or} \quad N_z = \overline{N}_{z_0} \tag{33a}$$

$$\delta U \ : \quad U = \overline{U}_0 \quad \text{or} \quad V_x = \overline{V}_{x_0} \tag{33b}$$

$$\delta V \ : \quad V = \overline{V}_0 \quad \text{or} \quad V_y = \overline{V}_{y_0} \tag{33c}$$

$$\delta\Phi \ : \quad \Phi = \overline{\Phi}_0 \quad \text{or} \quad T + M_t = \overline{T}_0 + \overline{M}_{t_0} \tag{33d}$$

$$\delta\Psi_y \ : \quad \Psi_y = \overline{\Psi}_{y_0} \quad \text{or} \quad M_y = \overline{M}_{y_0} \tag{33e}$$

$$\delta\Psi_x \ : \quad \Psi_x = \overline{\Psi}_{x_0} \quad \text{or} \quad M_x = \overline{M}_{x_0} \tag{33f}$$

$$\delta\Psi_\omega \ : \quad \Psi_\omega = \overline{\Psi}_{\omega_0} \quad \text{or} \quad M_\omega = \overline{M}_{\omega_0} \tag{33g}$$

The 7^{th} denotes the warping restraint boundary condition. When the warping of the cross section is restrained, $\Psi_\omega = 0$ and when the warping is not restrained, $M_\omega = 0$.

Eq.(32) is most general form for axial-flexural-torsional-shearing vibration and buckling of thin-walled composite beams. For general anisotropic materials, the dependent variables, U, V, W, Φ, Ψ_x, Ψ_y and Ψ_ω are fully-coupled implying that the beam undergoes a coupled behavior involving bending, extension, twisting, transverse shearing, and warping. The resulting coupling is referred to as sixfold coupled vibration and buckling. If all the coupling effects and the inertia coefficients are neglected as well as cross section is symmetrical with respect to both x- and the y-axes, Eq.(32) can be simplified to the uncoupled differential equations as

$$\begin{aligned}
(EA)_{com}W'' &= 0 && (34a)\\
(GA_y)_{com}(U'' + \Psi_y') + P^0U'' &= 0 && (34b)\\
(GA_x)_{com}(V'' + \Psi_x') + P^0V'' &= 0 && (34c)\\
\Big[(GJ_1)_{com} + P^0\frac{I_p}{A}\Big]\Phi'' - (GJ_2)_{com}\Psi_\omega' &= 0 && (34d)\\
(EI_y)_{com}\Psi_y'' - (GA_y)_{com}(U' + \Psi_y) &= 0 && (34e)\\
(EI_x)_{com}\Psi_x'' - (GA_x)_{com}(V' + \Psi_x) &= 0 && (34f)\\
(EI_\omega)_{com}\Psi_\omega'' + (GJ_2)_{com}\Phi' - (GJ_1)_{com}\Psi_\omega &= 0 && (34g)
\end{aligned}$$

From above equations, $(EA)_{com}$ represents axial rigidity, $(GA_x)_{com}$, $(GA_y)_{com}$ represent shear rigidities with respect to x and y axis, $(EI_x)_{com}$ and $(EI_y)_{com}$ represent flexural rigidities with respect to x- and y-axis, $(EI_\omega)_{com}$ represents warping rigidity, and $(GJ_1)_{com}$, $(GJ_2)_{com}$, $(GJ)_{com}$ represent torsional rigidities of thin-walled composite beams, respectively, written as

$$\begin{aligned}
(EA)_{com} &= E_{11} && (35a)\\
(EI_y)_{com} &= E_{22} && (35b)\\
(EI_x)_{com} &= E_{33} && (35c)\\
(EI_\omega)_{com} &= E_{44} && (35d)\\
(GA_y)_{com} &= E_{66} && (35e)\\
(GA_x)_{com} &= E_{77} && (35f)\\
(GA_\omega)_{com} &= E_{88} && (35g)\\
(GJ_1)_{com} &= E_{55} + E_{88} && (35h)\\
(GJ_2)_{com} &= E_{55} - E_{88} && (35i)\\
(GJ)_{com} &= 4E_{55} && (35j)
\end{aligned}$$

It is well known that the three distinct buckling modes, flexural buckling in the x- and y-direction, and torsional buckling, are identified in this case, and the corresponding buckling loads are given by orthotropy solution for a clamped beam boundary conditions [10]

$$P_x = \Big[\frac{(0.5l)^2}{\pi^2(EI_x)_{com}} + \frac{1}{(GA_x)_{com}}\Big]^{-1} \tag{36a}$$

$$P_y = \Big[\frac{(0.5l)^2}{\pi^2(EI_y)_{com}} + \frac{1}{(GA_y)_{com}}\Big]^{-1} \tag{36b}$$

$$P_\theta = \frac{A}{I_p}\Big[\big[\frac{(0.5l)^2}{\pi^2(EI_\omega)_{com}} + \frac{1}{(GA_\omega)_{com}}\big]^{-1} + (GJ)_{com}\Big] \tag{36c}$$

where P_x, P_y, P_θ are flexural buckling loads in the x- and y-direction, and torsional buckling load, respectively.

VI. FINITE ELEMENT FORMULATION

The present theory for thin-walled composite beams described in the previous section was implemented via a one-dimensional displacement-based finite element method. The generalized displacements are expressed over each element as a linear combination of the one-dimensional Lagrange interpolation function $\widehat{\phi_j}$ associated with node j and the nodal values

$$W = \sum_{j=1}^{n} w_j \widehat{\phi_j} \tag{37a}$$

$$U = \sum_{j=1}^{n} u_j \widehat{\phi_j} \tag{37b}$$

$$V = \sum_{j=1}^{n} v_j \widehat{\phi_j} \tag{37c}$$

$$\Phi = \sum_{j=1}^{n} \phi_j \widehat{\phi_j} \tag{37d}$$

$$\Psi_y = \sum_{j=1}^{n} \psi_{yj} \widehat{\phi_j} \tag{37e}$$

$$\Psi_x = \sum_{j=1}^{n} \psi_{xj} \widehat{\phi_j} \tag{37f}$$

$$\Psi_\omega = \sum_{j=1}^{n} \psi_{\omega j} \widehat{\phi_j} \tag{37g}$$

Substituting these expressions into the weak statement in Eq.(28), the finite element model of a typical element can be expressed as

$$([K] - P^0[G] - \omega^2[M])\{\Delta\} = \{0\} \tag{38}$$

where $[K], [M]$ are the element stiffness matrix, the element mass matrix and given in Ref.[24]. The element geometric stiffness matrix $[G]$ are defined by

$$[G] = \begin{bmatrix} G_{11} & G_{12} & G_{13} & G_{14} & G_{15} & G_{16} & G_{17} \\ & G_{22} & G_{23} & G_{24} & G_{25} & G_{26} & G_{27} \\ & & G_{33} & G_{34} & G_{35} & G_{36} & G_{37} \\ & & & G_{44} & G_{45} & G_{46} & G_{47} \\ & & & & G_{55} & G_{56} & G_{57} \\ & & & & & G_{66} & G_{67} \\ \text{sym.} & & & & & & G_{77} \end{bmatrix} \tag{39}$$

The explicit forms of $[G]$ are given by

$$G_{ij}^{22} = G_{ij}^{33} = \int_0^l \psi_i' \psi_j' dz \tag{40a}$$

$$G_{ij}^{24} = \int_0^l y_p \psi_i' \psi_j' dz \tag{40b}$$

$$G_{ij}^{34} = -\int_0^l x_p \psi_i' \psi_j' dz \tag{40c}$$

$$G_{ij}^{44} = \int_0^l \frac{I_p}{A} \psi_i' \psi_j' dz \tag{40d}$$

All other components are zero.

In Eq.(38), $\{\Delta\}$ is the eigenvector of nodal displacements corresponding to an eigenvalue

$$\{\Delta\} = \{W \ U \ V \ \Phi \ \Psi_y \ \Psi_x \ \Psi_\omega\}^{\mathrm{T}} \tag{41}$$

VII. NUMERICAL EXAMPLES

For verification purpose, the buckling behavior and free vibration of a cantilever isotropic mono-symmetric channel section beam, as shown in Fig.2, with length l =2m under axial force at the centroid is performed. Throughout the numerical examples, ten quadratic elements with three nodes are used. The material properties are assumed to be: $E = 0.3$GPa , $G = 0.115$GPa , $\rho = 7850$kg/m^3. The buckling loads and natural frequencies are evaluated and compared with numerical results of Kim et al.[27] which is based on dynamic stiffness formulation and ABAQUS solutions in Table I. The present results are in a good agreement with those by Kim et al.[27].

In the next example, a simply-supported composite I-beam with a span of 6.0m under axial force applied to the centroid is analyzed. A doubly symmetric I-section of 600mm wide flange and 600mm deep web is considered. The flanges and web are made of four plies with each ply 7.5mm in thickness. The material is graphite-epoxy whose layer properties are defined: $E_1 = 144$GPa , $E_2 = 9.65$GPa , $G_{12} = G_{13} = 4.14$GPa , $G_{23} = 3.45$GPa , $\nu_{12} = 0.3$. Plane stress assumption ($\sigma_s = 0$) is made in the analysis. The critical buckling loads obtained from the present analysis are given in Table II, along with the finite element results of Machado and Cortinez [16] and Back and Will [19]. It is observed that the present results are in good agreement with the solutions in Refs.[16,19] for all cases of lay-ups.

To demonstrate the accuracy and validity of this study further, a cantilever symmetrically laminated mono-symmetric I-beam with length $l = 1$m under axial load at the centroid is considered. Following dimensions for the beam are used: the height, top and bottom flange widths are 50mm, 30mm and 50mm, respectively. The flanges and web are made of sixteen layers with each layer 0.13mm in thickness. All computations are carried out for the glass-epoxy materials with the following material properties: $E_1 = 53.78$GPa , $E_2 = 17.93$GPa , $G_{12} = G_{13} = 8.96$GPa , $G_{23} = 3.45$GPa , $\nu_{12} = 0.25$. The comparison of the critical buckling loads among the proposed finite element solution, the analytical approach by Kim et al. [21] are given in Table III for different stacking sequences. The present finite element solution again indicates good agreement with the analytical solution and ABAQUS results for all lamination schemes considered.

In order to investigate the effects of fiber orientation and shear deformation on the critical buckling loads and the mode shapes as well as load-frequency interaction curves, thin-walled composite I-beams with different span-to-height ratios under axial load at the centroid are considered. The geometry and stacking sequences of I-section are shown in Fig.3, and the following engineering constants are used

$$E_1/E_2 = 25, G_{12}/E_2 = 0.6, G_{13} = G_{12} = G_{23}, \nu_{12} = 0.25 \tag{42}$$

For convenience, the following nondimensional buckling load and natural frequency are used

$$\overline{P} = \frac{Pl^2}{b_3^3 t E_2} \tag{43}$$

$$\bar{\omega} = \frac{\omega l^2}{b_3}\sqrt{\frac{\rho}{E_2}} \tag{44}$$

The flanges and web are considered as antisymmetric angle-ply laminates $[\theta/-\theta]$, (Fig.3a). For this lay-up, all the coupling stiffnesses are zero, but E_{35} and E_{38} do not vanish due to unsymmetric stacking sequence of the flanges and web. As the first example, the stacking sequence at two specific fiber angle $\theta = 0°$ and $30°$ is considered to investigate the effects of axial force and shear deformation on the fundamental natural frequency. Fig.4 shows the interaction diagram between flexural-torsional buckling and natural frequency with span-to-height ratio $l/b_3 = 10$. By using a linear combination of the one-dimensional Lagrange and Hermite-cubic interpolation function in finite element formulation [22], the load-frequency interaction curves obtained from previous research [25] based on the classical beam theory are also displayed. It can be seen that the change in the natural frequency due to axial force is noticeable. The natural frequency diminishes when the axial force changes from tensile to compressive, as expected. It is obvious that the natural frequency decreases with the increase of axial force, and the decrease becomes more quickly when the axial force is close to critical buckling load. Moreover, this decrease is more pronounced with fiber angle $\theta = 0°$ when the shear effects are included in the analysis. With $\theta = 0°$ and $30°$, at about $\overline{P}$=36.165 and 12.806, the natural frequencies become zero which implies that at these loads, flexural-torsional bucklings occur as a degenerate case of natural vibration at zero frequency. It is from Fig.4 that explains the duality between the critical flexural-torsional buckling load and the fundamental natural frequency.

The next example is the same as before except that in this case, the fiber angle is rotated in the flanges and web (Fig.3a). The critical buckling loads by the finite element analysis (FEM) and the orthotropy solutions, which neglects the coupling effects of E_{35}, E_{38}, from Eqs.(36a)-(36c) are given in Fig.5. The results with no shear effects calculated from previous paper [22]. As expected, for classical beam model, the critical buckling loads decrease monotonically with the increase of fiber angle. However, for present model, after P_{cr} reaches maximum value around $\theta = 10°$, it decreases. This local maximum occurs because at low fiber angle, large shear effects reduce flexural stiffnesses. It is interesting to note that the shear effects are negligibly small even for the lower span-to-height ratio ($l/b_3 = 10$), especially in the interval $\theta \in [30°, 90°]$. This trend can be explained that the flexural stiffnesses decrease significantly with the increasing fiber angle, and thus, the relative shear effects become smaller for higher fiber angles. Due to coupling stiffnesses, the orthotropy solution might not be accurate. However, as fiber angle increases, the coupling effects coming from the material anisotropy become negligible. Therefore, it can be seen in Fig.5, for all fiber angles, the critical buckling loads by the finite element analysis exactly correspond to the flexural buckling loads in y-direction. It can be explained partly by the typical mode shapes with the fiber angle $\theta = 30°$ in Fig.6. It is indicated that the simple orthotropy solution is sufficiently accurate for this lay-up.

To investigate the coupling and shear effects further, the same configuration with the previous example except the lay-up is considered. The bottom flange is considered as $[\theta_2]$, while the top flange and web are [0/45], respectively

(Fig.3b). For this lay-up, the coupling stiffnesses $E_{16}, E_{17}, E_{18}, E_{36}, E_{37}$ and E_{68} become no more negligibly small. Fig.7 displays the effects of shear deformation on the critical buckling loads with two different ratios. For $l/b_3 = 25$, since the shear effects are negligible, the solutions of two models nearly coincide. However, for lower span-to-height ratio ($l/b_3 = 5$), it is noticed that discarding shear effects again leads to an overprediction of the critical buckling loads for all fiber angles especially in the range of $\theta \in [0^\circ, 30^\circ]$. The results by orthotropy solution and the finite element analysis with $l/b_3 = 5$ are shown in Fig.8. The buckling mode shapes with various fiber angles $\theta = 0^\circ, 15^\circ$ and 75° are illustrated in Figs.9-11. Three types of mode shapes can be seen. Relative measures of axial, flexural displacements, torsional and shearing rotations show that, at $\theta = 0^\circ$ when the beam is buckling exhibits fourfold coupled mode (the flexural mode in y-direction, torsional mode and corresponding shearing mode), whereas, at $\theta = 15^\circ$, the beam displays three further mode (axial mode, the flexural mode in x-direction and corresponding shearing mode). Due to small out-of-plane displacement W (Fig.10), the resulting mode shape is referred to as sixfold coupled mode. It is from this sixfold coupled mode that highlights the influence of coupling and shear effects on the buckling behavior of thin-walled composite beams. This response is never observed in the classical beam model [22] because the shear effects are not present. As fiber angle increases, since the coupling stiffnesses decrease, the buckling mode shape becomes predominantly torsional mode as shown in Fig.11. Consequently, the critical buckling loads by the finite element analysis exactly correspond to the torsional buckling loads of orthotropy solution. This fact explains as the fiber angle changes, for lower span-to-height ratio, the orthotropy solutions disagree with the finite element solutions as anisotropy of the beam gets higher. That is, the orthotropy solution is no longer valid for unsymmetrically laminated beams, and sixfold coupled flexural-torsional-shearing buckling should be considered even for a doubly symmetric cross-section.

Finally, the effects of span-to-height ratio (l/b_3) and modulus ratio (E_1/E_2) on the critical buckling loads of a simply supported beam are investigated. The stacking sequence of the flanges and web are $[0/90]_s$, (Fig.3c). For this lay-up, all the coupling stiffnesses vanish and thus, the critical buckling loads exactly correspond to the flexural buckling loads in y-direction. It is evident from Fig.12 that the shear-deformable beam theory is very effective in a relatively large region up to the point where span-to-height ratio reaches value of $l/b_3 = 20$. For this reason, a span-to-height ratio $l/b_3 = 5$ is chosen to show effect of modulus ratio on the the critical buckling loads. The critical buckling loads increase as modulus ratio increase in Fig.13. It is obvious that the omission of shear effects causes an overestimation of the critical buckling loads with increasing orthotropy (E_1/E_2).

VIII. CONCLUDING REMARKS

A analytical model based on shear-deformable beam theory is presented to study the flexural-torsional buckling of thin-walled composite beams under axial load. This model is capable of predicting accurately the critical buckling loads and corresponding mode shapes for various configuration. All of the possible buckling mode shapes including the flexural mode in the x- and y-direction, the torsional mode, and fully coupled flexural-torsional-shearing mode are included in the analysis. The shear effects become significant for lower span-to-height ratio. The orthotropy solution is accurate for lower degrees of material anisotropy, but, becomes inappropriate as the anisotropy of the beam gets higher, and fully coupled equations should be considered for accurate analysis of thin-walled composite beams. The present model is found to be appropriate and efficient in analyzing buckling problem of thin-walled composite beams under axial load.

Acknowledgments

The support of the research reported here by Seoul R&BD Program through Grant GR070033 is gratefully acknowledged. The authors also would like to thank the anonymous reviewers for their suggestions in improving the standard of the manuscript.

References

[1] Vlasov VZ. Thin-walled elastic beams. 2nd Edition. Jerusalem, Israel: Israel Program for Scientific Translation, 1961.

[2] Gjelsvik A. The theory of thin-walled bars. New York: John Wiley and Sons Inc., 1981.

[3] Timoshenko SV, Gere JM. Theory of Elastic Stability. New York: McGraw-Hill, 1961.

[4] Trahair NS. Flexural-torsional buckling of structures. London: CRC Press, 1993.

[5] Pandey MD, Kabir MZ and Sherbourne AN. Flexural-torsional stability of thin-walled composite I-section beams. Compos Eng 1995; 5(3):321-342.

[6] Lin ZM, Polyzois D and Shah A. Stability of thin-walled pultruded structural members by the finite element method. Thin-Walled Struct 1996; 24(1):1-18.

[7] Shield CK and Morey TA. Kinematic theory of open and closed section thin-walled composite beams. J Eng Mech 1997; 123(10):1070-1081.

[8] Kollar LP. Flexural-torsional buckling of open section composite columns with shear deformation. Int J Solids Struct 2001; 38(42-43):7525-7541.

[9] Kollar LP. Flexural-torsional vibration of open section composite columns with shear deformation. Int J Solids Struct 2001; 38(42-43):7543-7558.

[10] Kollar LP and Springer GS. Mechanics of composite structure. Cambridge University Press, 2003.

[11] Davalos JF, Qiao P and Salim HA. Flexural-torsional buckling of pultruded fiber reinforced plastic composite I-beams: experimental and analytical evaluations. Compos Struct 1997; 38(1-4):241-250.

[12] Qiao P, Zou G and Davalos JF. Flexural-torsional buckling of fiber-reinforced plastic composite cantilever I-beams. Compos Struct 2003; 60(2):205-217.

[13] Shan L and Qiao P. Flexural-torsional buckling of fiber-reinforced plastic composite open channel beams. Compos Struct 2005; 68(2):211-224.

[14] Librescu L and Song 0. Thin-walled Composite Beams. Springer, 2006.

[15] Cortinez VH and Piovan MT. Vibration and buckling of composite thin-walled beams with shear deformability. J Sound Vib 2002; 258(4-5):701-723.

[16] Machado SP and Cortinez VH. Non-linear model for stability of thin-walled composite beams with shear deformation. Thin-Walled Struct 2005; 43(10):1615-1645.

[17] Cortinez VH and Piovan MT. Stability of composite thin-walled beams with shear deformability. Comput Struct 2006; 84(15-16):978-990.

[18] Piovan MT and Cortinez VH. Mechanics of shear deformable thin-walled beams made of composite materials. Thin-Walled Struct 2007; 45(1):37-62

[19] Back SY and Will KM. Shear-flexible thin-walled element for composite I-beams. Eng Struct 2007; 30(5): 1447-1458

[20] Kim NI, Shin DK and Kim MY. Improved flexural-torsional stability analysis of thin-walled composite beam and exact stiffness matrix. Int J Mech Sci 2007; 49(8):950-969.

[21] Kim NI, Shin DK and Kim MY. Flexural-torsional buckling loads for spatially coupled stability analysis of thin-walled composite columns. Adv Eng Softw 2008; 39(12):949-961.

[22] Lee J and Kim S. Flexural-torsional buckling of thin-walled I-section composites. Comput Struct 2001; 79(10):987-995.

[23] Lee J. Flexural analysis of thin-walled composite beams using shear-deformable beam theory. Compos Struct 2005; 70(2):212-222.

[24] Vo TP and Lee J. On sixfold coupled vibrations of thin-walled composite box beams. Compos Struct 2008; In Press.

[25] Vo TP and Lee J. Flexural-torsional coupled vibration of axially loaded thin-walled open-section composite beams. Thin-walled Struct 2008, submitted.

[26] Jones RM. Mechanics of composite materials. New York: Hemisphere Publishing Corp., 1975.

[27] Kim MY, Kim NI and Yun HT. Exact dynamic and static stiffness matrices of shear deformable thin-walled beam-columns. J Sound Vib 2003; 267(1):29-55.

CAPTIONS OF TABLES

Table I: The bucking loads and natural frequencies a cantilever isotropic mono-symmetric channel section beam.

Table II: Critical bucking loads of a simply supported doubly symmetric composite I-beam (10^6N).

Table III: Critical bucking loads of a cantilever mono-symmetric composite I-beam (N).

CAPTIONS OF FIGURES

Figure 1: Definition of coordinates and generalized displacements in thin-walled open sections.

Figure 2: Isotropic mono-symmetric channel section for verification.

Figure 3: Geometry and stacking sequences of thin-walled composite I-beam.

Figure 4: The effect of axial force on the fundamental natural frequency with the fiber angle 0° and 30° in the flanges and web of a clamped composite beam with $l/b_3 = 10$.

Figure 5: Variation of the critical buckling loads with respect to fiber angle change in the flanges and web of a clamped composite beam with $l/b_3 = 10$.

Figure 6: Mode shapes of the flexural-shearing components for $P_{cr} = 12.806$ with the fiber angle 30° in the flanges and web of a clamped composite beam with $l/b_3 = 10$.

Figure 7: Variation of the critical buckling loads with respect to fiber angle change in the bottom flange of clamped composite beams with $l/b_3 = 5$ and $l/b_3 = 25$.

Figure 8: Variation of the critical buckling loads with respect to fiber angle change in the bottom flange of a clamped composite beam with $l/b_3 = 5$.

Figure 9: Mode shapes of the flexural-torsional-shearing components for $P_{cr} = 16.563$ with the fiber angle 0° in the bottom flange of a clamped composite beam with $l/b_3 = 5$.

Figure 10: Mode shapes of the flexural-torsional-shearing components for $P_{cr} = 19.059$ with the fiber angle 15° in the bottom flange of a clamped composite beam with $l/b_3 = 5$.

Figure 11: Mode shapes of the torsional-shearing components for $P_{cr} = 2.234$ with the fiber angle 75° in the bottom flange of a clamped composite beam with $l/b_3 = 5$.

Figure 12: Variation of the critical buckling loads of a simply supported composite beam with respect to span-to-height ratio change.

Figure 13: Variation of the critical buckling loads with respect to modulus ratio change of a simply supported composite beam with $l/b_3 = 5$.

TABLE I The bucking loads and natural frequencies a cantilever isotropic mono-symmetric channel section beam.

Mode	Buckling loads (N)			Natural frequencies (rad/s)^2		
	Ref.[27]		Present	Ref.[27]		Present
	ABAQUS	With shear		ABAQUS	With shear	
1	0.027	0.028	0.026	13.789	14.001	12.977
2	0.334	0.331	0.334	111.840	113.100	113.440
3	0.704	0.696	0.707	191.160	190.080	190.567
4	1.065	1.074	1.084	255.100	256.670	263.999

TABLE II Critical bucking loads of a simply supported doubly symmetric composite I-beam (10^6N).

Lay-ups	Ref.[16]		Ref.[19]		Present
	No shear	With shear	ABAQUS	With shear	
$[0]_4$	42.11	33.18	30.78	28.85	30.38
$[30/-30]_s$			13.06	13.17	13.17
$[45/-45]_s$	4.45	4.44	4.40	4.41	4.41
$[60/-60]_s$			2.89	2.89	2.88
$[0/90]_s$	22.57	19.84	20.41	20.63	20.63

TABLE III Critical bucking loads of a cantilever mono-symmetric composite I-beam (N).

Lay-ups	Ref.[21]		Present
	ABAQUS	No shear	
$[0]_{16}$	2969.7	2998.2	2993.2
$[15/-15]_{4s}$	2790.9	2811.8	2803.6
$[30/-30]_{4s}$	2190.6	2199.7	2184.7
$[45/-45]_{4s}$	1558.9	1561.9	1546.0
$[60/-60]_{4s}$	1239.4	1241.3	1227.8
$[75/-75]_{4s}$	1132.2	1134.5	1126.7
$[0/90]_{4s}$	2101.5	2113.9	2100.6

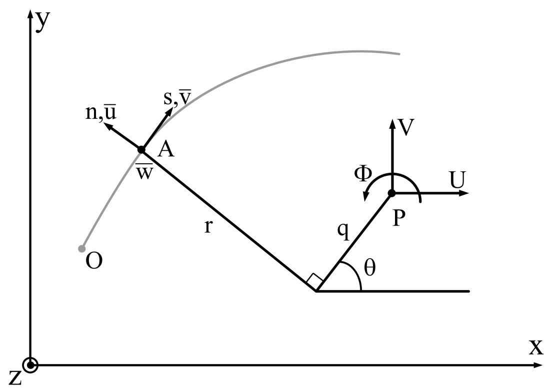

FIG. 1 Definition of coordinates and generalized displacements in thin-walled open sections.

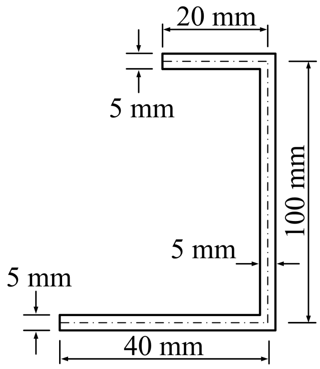

FIG. 2 Isotropic mono-symmetric channel section for verification.

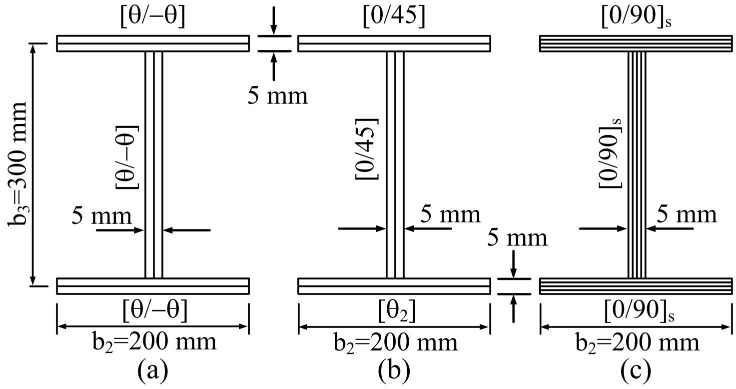

FIG. 3 Geometry and stacking sequences of thin-walled composite I-beam.

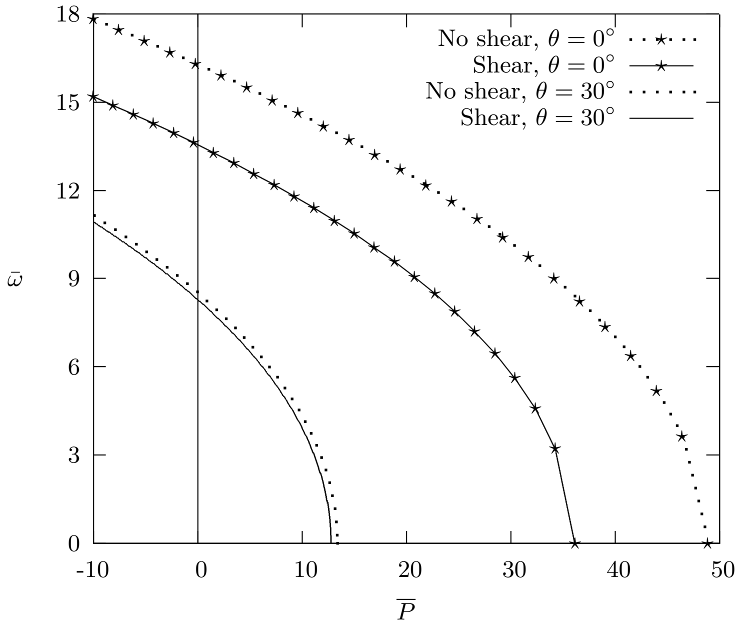

FIG. 4 The effect of axial force on the fundamental natural frequency with the fiber angle 0° and 30° in the flanges and web of a clamped composite beam with $l/b_3 = 10$.

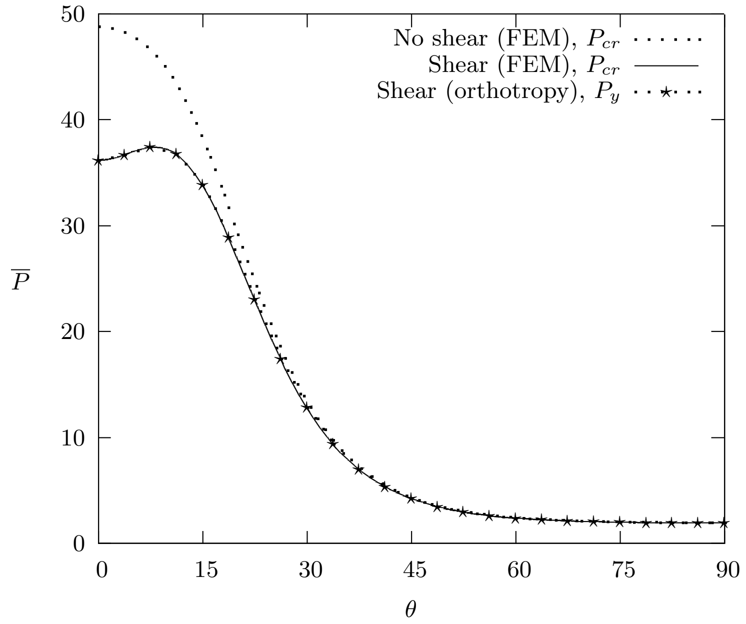

FIG. 5 Variation of the critical buckling loads with respect to fiber angle change in the flanges and web of a clamped composite beam with $l/b_3 = 10$.

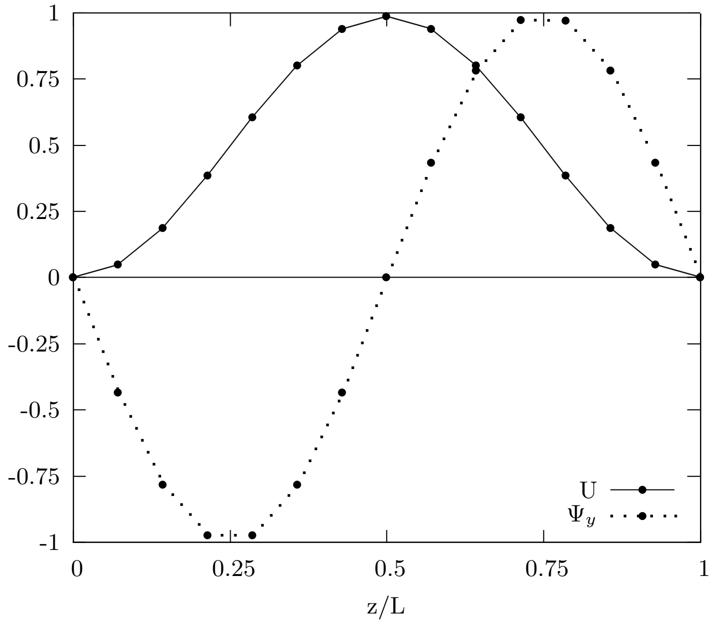

FIG. 6 Mode shapes of the flexural-torsional-shearing components for $P_{cr} = 12.806$ with the fiber angle 30° in the flanges and web of a clamped composite beam with $l/b_3 = 10$.

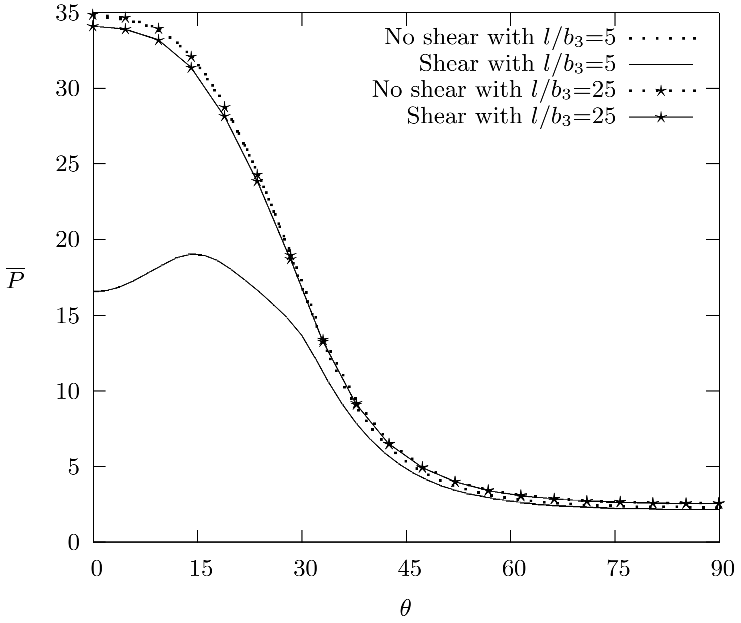

FIG. 7 Variation of the critical buckling loads with respect to fiber angle change in the bottom flange of clamped composite beams with $l/b_3 = 5$ and $l/b_3 = 25$.

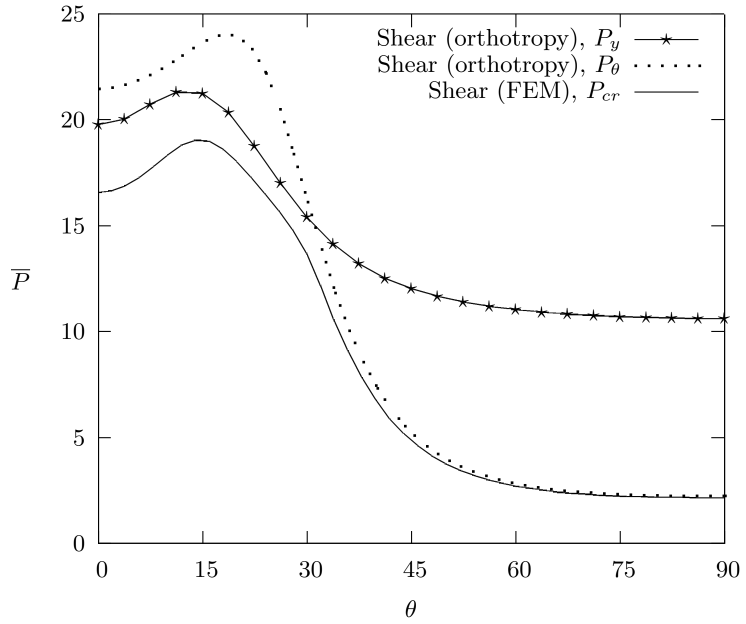

FIG. 8 Variation of the critical buckling loads with respect to fiber angle change in the bottom flange of a clamped composite beam with $l/b_3 = 5$.

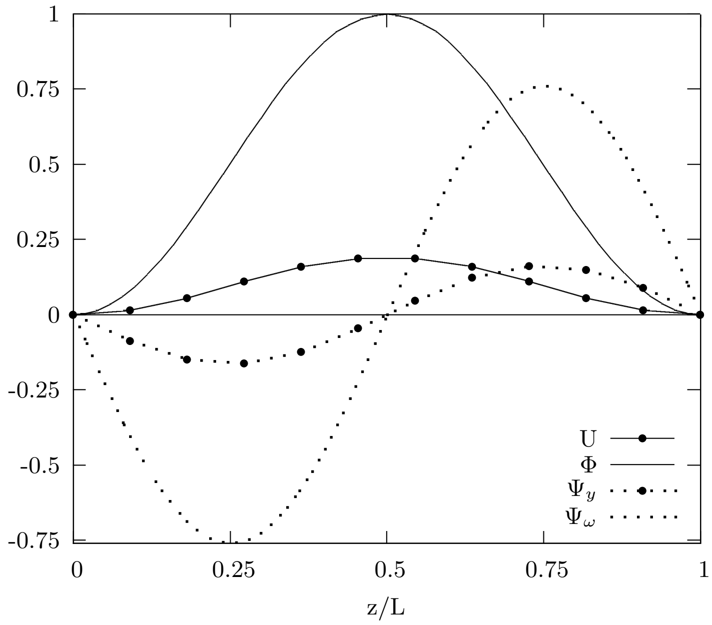

FIG. 9 Mode shapes of the flexural-torsional-shearing components for $P_{cr} = 15.563$ with the fiber angle 0° in the bottom flange of a clamped composite beam with $l/b_3 = 5$.

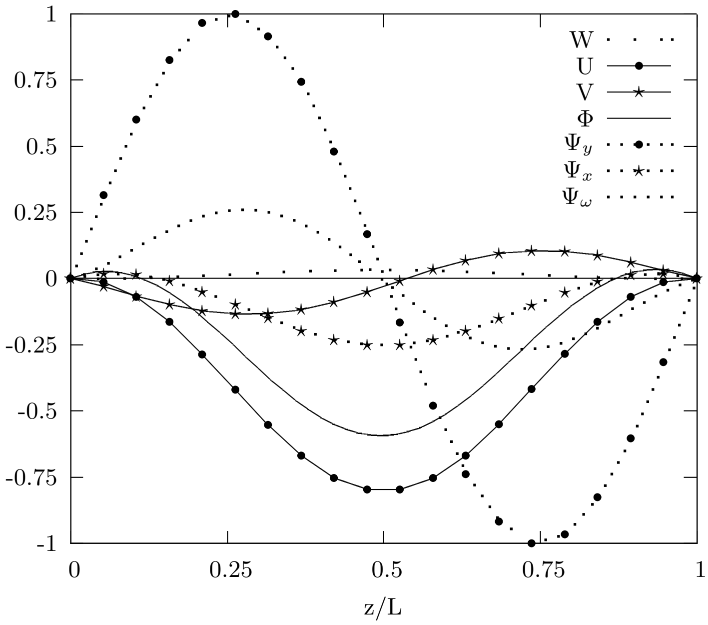

FIG. 10 Mode shapes of the flexural-torsional-shearing components for $P_{cr} = 19.059$ with the fiber angle 15° in the bottom flange of a clamped composite beam with $l/b_3 = 5$.

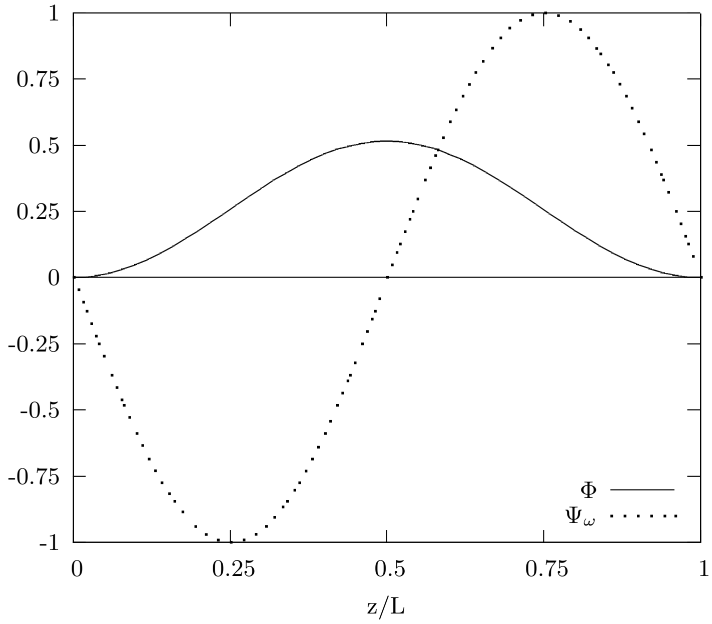

FIG. 11 Mode shapes of the torsional-shearing components for $P_{cr} = 2.234$ with the fiber angle 75° in the bottom flange of a clamped composite beam with $l/b_3 = 5$.

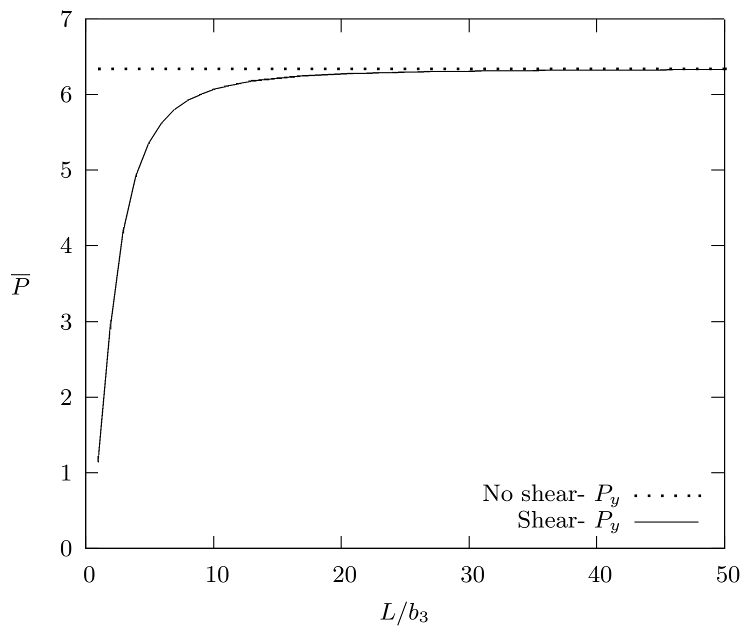

FIG. 12 Variation of the critical buckling loads of a simply supported composite beam with respect to span-to-height ratio change.

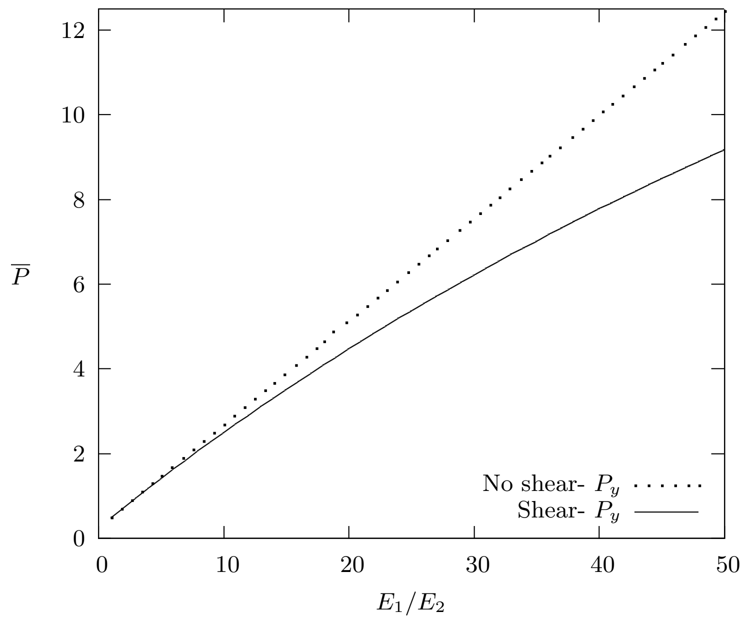

FIG. 13 Variation of the critical buckling loads with respect to modulus ratio change of a simply supported composite beam with $l/b_3 = 5$.